International Journal of Pharmaceutics 617 (2022) 121618

Contents lists available at ScienceDirect

International Journal of Pharmaceutics

journal homepage: www.elsevier.com/locate/ijpharm

Sphingomyelin nanosystems decorated with TSP-1 derived peptide targeting senescent cells

Raneem Jatal [a,b,1], Sofia Mendes Saraiva [a,c,d,1], Carlos Vázquez-Vázquez [e], Eric Lelievre [b], Olivier Coqueret [b], Rafael López-López [c,f], María de la Fuente [a,c,f,g,*]

[a] Nano-Oncology and Translational Therapeutics Group, Health Research Institute of Santiago de Compostela (IDIS), SERGAS, 15706 Santiago de Compostela, Spain
[b] Paul Papin ICO Cancer Center, INSERM 1232, Angers University, 49100 Angers, France
[c] Biomedical Research Networking Center on Oncology (CIBERONC), 28029 Madrid, Spain
[d] CPIRN-IPG- Center of Potential and Innovation of Natural Resources, Polytechnic Institute of Guarda, Av. Dr. Francisco de Sá Carneiro, No. 50, 6300-559 Guarda, Portugal
[e] Laboratory of Magnetism and Nanotechnology (NANOMAG), Faculty of Chemistry, Department of Physical Chemistry, Universidad de Santiago de Compostela, 15706 Santiago de Compostela, Spain
[f] Translational Medical Oncology Group (ONCOMET), Health Research Institute of Santiago de Compostela (IDIS), SERGAS, 15706 Santiago de Compostela, Spain
[g] DIVERSA Technologies, 15782 Santiago de Compostela, Spain

ARTICLE INFO

Keywords:
Cellular senescence
TSP-1
Sphingomyelin nanoemulsions

ABSTRACT

Senescent cells accumulation can contribute to the development of several age-related diseases, including cancer. Targeting and eliminating senescence cells, would allow the development of new therapeutic approaches for the treatment of different diseases. The 4N1Ks peptide, a 10 amino acid peptide derived from TSP1 protein, combines both features by targeting the CD47 receptor present in the surface of senescent cells and demonstrating senolytic activity, thereby representing a new strategy to take into account. Nonetheless, peptide drugs are known for their biopharmaceutical issues, such as low short half-life and tendency to aggregate, which reduces their bioavailability and limits their therapeutic potential. In order to overcome this problem, herein we propose the use of biodegradable and biocompatible sphingomyelin nanosystems (SNs), decorated with this peptide for the targeting of senescent cells. In order to efficiently associate the 4N1Ks peptide to the nanosystems while exposing it on their surface for an effective targeting of senescent cells, the 4N1Ks peptide was chemically conjugated to a PEGylated hydrophobic chain. The resulting SNs-4N1Ks (SNs-Ks), were extensively characterized for their physicochemical properties, by dynamic light scattering, multiple-angle dynamic light scattering, nanoparticle tracking analysis and atomic force microscopy. The SNs-Ks demonstrated suitable features in terms of size (~100 nm), association efficiency (87.2 ± 6.9%) and stability in different biorelevant media. Cell toxicity experiments in MCF7 cancer cells indicated an improved cytotoxic effect of SNs-Ks, decreasing cancer cells capacity to form colonies, with respect to free peptide, and an improved hemocompatibility. Lastly, senescence escape preliminary experiments demonstrated the improvement of SNs-Ks senolytic activity of in chemotherapy-induced senescence model of breast cancer cells. Therefore, these results demonstrate for the first time the potential of the combination of SNs with 4N1Ks peptide for the development of innovative senolytic therapies to battle cancer.

Abbreviations: SM, sphingomyelin; VitE, vitamin E; SNs, sphingomyelin nanosystems; Ks, C18-PEG-4N1Ks; DLS, dynamic light scattering; NTA, Nanoparticle tracking analysis; MADLS, multi angle dynamic light scattering; AFM, atomic force microscopy; MW, molecular weight; MWCO, membrane molecular-weight cut-off; MetOH, methanol; EtOH, ethanol; RT, room temperature; PdI, polydispersity index; PBS, phosphate buffer saline; FBS, fetal bovine serum; AE, association efficiency; IV, intravenous; SASP, senescent-associated secretory phenotypes; MTT, tetrazolium bromide; TEM, Transmission Electron Microscopy.

* Corresponding author at: Nano-Oncology and Translational Therapeutics Group, Health Research Institute of Santiago de Compostela (IDIS), SERGAS, 15706 Santiago de Compostela, Spain.

E-mail addresses: raneem-j@aucegypt.edu (R. Jatal), sofiasaraiva@ipg.pt (S. Mendes Saraiva), carlos.vazquez.vazquez@usc.es (C. Vázquez-Vázquez), eric.lelievre@univ-angers.fr (E. Lelievre), olivier.coqueret@univ-angers.fr (O. Coqueret), maria.de.la.fuente.freire@sergas.es, maria.fuente@usc.es (M. de la Fuente).

[1] Both authors share first authorship.

https://doi.org/10.1016/j.ijpharm.2022.121618
Received 16 October 2021; Received in revised form 8 February 2022; Accepted 21 February 2022
Available online 24 February 2022

1. 1. Introduction

Peptides' potency and high value to medicine has pushed them to come a long way. Currently, there are 86 peptide drugs on the market for the management of several human diseases (Durán-Lobato et al., 2021). Among small-drugs and biologicals, in 2019 peptide drugs accounted for 5% of the pharmaceutical market, with sales above $50 billion (Muttenthaler et al., 2021). By 2025 it is expected that the protein market will reach $155.06 billion ("Therapeutic Proteins Global Market Report 2021: COVID-19 Impact and Recovery to 2030," n.d.). However, peptide delivery presents several limitations such as short half-life and low bioavailability due to enzymatic degradation, instability and fast renal clearance; as well as immunogenicity, which limits their full exploitation (Bruno et al., 2013; Fosgerau and Hoffmann, 2015). Nanomedicine, among other strategies, can overcome peptides' stability issues, improve their half-life and bioavailability, and consequently their therapeutic effect (Durán-Lobato et al., 2021; Fosgerau and Hoffmann, 2015). Among the different types of nanocarriers, liposomes, polymeric nanoparticles and solid lipid nanoparticles have been widely used for peptide delivery (Solaro et al., 2010). Depending on the intended application, peptides can be either encapsulated in the nanoparticles core or associated on their surface (Jeong et al., 2018; Pudlarz and Szemraj, 2018). In this work, we aim at decorating the surface of nanocarriers with 4N1Ks peptide for the targeting of CD47 receptor, expressed on the surface of the targeted senescent cells.

Milanovic *et al.* has recently contradicted the concept of irreversible cell cycle arrest as the main feature of cellular senescence, by demonstrating that chemotherapy-induced senescent cells can escape this stage turning into a more aggressive form of cancer cells (cancer stem cells) with enhanced growth potential (Milanovic et al., 2018). The accumulation of these cells due to the immune surveillance system failure, provides a proinflammatory niche that results in several age-related diseases, including cancer. In addition, it was demonstrated that tumor sites rich in senescent cells are directly linked to cancer relapse (Milanovic et al., 2018; Saleh et al., 2019). In this sense, the elimination of senescent cells using senolytic drugs has been the centre of attention of several researchers to improve cancer and age-related diseases outcome (Paez-Ribes et al., 2019; Wissler Gerdes et al., 2020; Zhu et al., 2015). Nowadays there are several drugs described in literature for their senolytic activity for cancer and other age-related diseases. Dasatinib, quercetin and rapamycin are some examples of senolytic drugs currently under clinical evaluation (Borghesan et al., 2020). In addition, considering that cellular senescence is a highly dynamic biological phenomenon, great efforts are being made to find senescence specific markers which will allow the development of senotherapies specifically targeted to these cells. In this regard, we have recently shown that homotrimer glycoprotein TSP-1/CD47 receptor is able to avoid senescence escape in chemotherapy-induced colon and breast cancer cells by inhibiting self-renewal and cell proliferation (Guillon et al., 2019). We have also shown that 4N1Ks, a 10 amino acid peptide derived from the C-terminal domain of TSP-1, also has the ability to prevent senescent cells escape by promoting autophagy in senescent and cancer cells (Jatal et al., 2021). Maintaining the senolytic activity while decreasing the molecular weight (MW) of the therapeutic molecule is a great advantage since peptides are cheaper to synthesize, present lower immunogenicity and enhanced tissue penetration in comparison to high MW proteins.

To the best of our knowledge, among the different senescence therapeutic drugs described in the literature, up to date, there are only a few publications referring to the use of nanomedicine for targeting cellular senescence (Agostini et al., 2012; Ekpenyong-Akiba et al., 2019; Ke et al., 2018; Lewinska et al., 2020; Muñoz-Espín et al., 2018; Thapa et al., 2017). Most of these consist of inorganic (silica, calcium carbonate, iron oxide, molybdenum) drug delivery systems that exploit the characteristic β-galactosidase activity of the senescent cells to achieve a controlled intracellular delivery of the senolytic drugs as navitoclax (Muñoz-Espín et al., 2018). Quercetin and CD9 monoclonal antibody functionalized inorganic nanoparticles are other strategies exploited for senescent cells targeting (Lewinska et al., 2020; Thapa et al., 2017).

In this study we propose the association of 4N1Ks peptide to nanoemulsions composed of sphingomyelin, which is present in cell membranes, and vitamin E, which has been extensively used in several formulations intended for clinical, and characterized for a good biodegradability and versatility for association and encapsulation of a variety of therapeutic molecules (Bouzo et al., 2021, 2020; Díez-Villares et al., 2021b, 2021a; Nagachinta et al., 2020b, 2020a). In addition, our previous works have shown that the sphingomyelin nanosystems (SNs) prepared by the simple and straightforward injection method present a great colloidal stability, low toxicity and high cell internalization (Bouzo et al., 2021, 2020). In order to incorporate 4N1Ks peptide into our nanosystem structure but still presenting it on their surface, our strategy was to chemically conjugate the peptide to a lipid (C18)-PEG (polyethylene glycol) derivative. We have previously observed that by using this strategy with another peptide we could improve the targeting of metastatic colorectal cancer cells (Bouzo et al., 2021).

While the stearic acid chain would allow the anchorage of the peptide to the SNs structure, the PEG moiety could reduce possible interactions with blood components like proteins (opsonisation), providing 'stealth' properties to nanosystems (Berrecoso et al., 2020). An extensive physicochemical characterization of the peptide nanocarriers was performed through different methods. Their effect on cancer cells viability and colony forming capacity was studied *in vitro* breast cancer cells and a chemotherapy-induced senescence model was used in a preliminary study to determine the capacity of the peptide-functionalized SNs to eliminate senescence cells.

2. 2. Materials and methods

2.1. Materials

Vitamin E (VitE, DL-α-Tocopherol) was purchased from Calbiochem (Merck-Millipore, Darmstadt, Germany). Sphingomyelin (SM, Lipoid E SM) was kindly provided by Lipoid GmbH (Ludwigshafen, Germany). C18-PEG-4N1Ks was synthesised by Covalab (Bron, France). HPLC grade Acetonitrile (ACN) and Ethanol (EtOH), Dimethyl sulfoxide (DMSO) were purchased from Acros Organics (country). Methanol (MetOH) was purchased from Merck (Darmstadt, Germany). Trifluoroacetic acid (TFA) and MTT (3-(4,5-Dimethyl-2-thiazolyl)-2,5-diphenyl-2H-tetrazolium Bromide) were provided by Sigma-Aldrich (Madrid, Spain). RPMI cell culture medium, Fetal bovine serum (FBS) and Doxorubicin hydrochloride (≥98%) were purchased from CAYMAN Chemical (Michigan, USA). All other chemicals used were HPLC or UPLC purity grade.

2.2. Preparation of SNs and association of 4N1Ks

SNs were prepared by the straightforward and very simple ethanol injection method, as previously reported by our research group (Bouzo et al., 2021; Nagachinta et al., 2020b). In short, VitE and SM were dissolved in ethanol at a concentration of 200 mg/mL and 40 mg/mL, respectively. Next, VitE and SM solutions were subsequently mixed to obtain a mass ratio of 1:0.1 (V:SM), corresponding to 5 mg of vitamin E. The resulting volume was completed up to 100 μL with ethanol and then injected into 1 mL of ultrapure water under continuous magnetic stirring (<10% of ethanol in the final formulation).

SNs associating 4N1Ks on the surface were prepared as follows. Initially, 4N1Ks was first modified by covalently linking it with a PEGylated-lipid containing a carboxyl group (C_{18}-PEG_6-COOH) resulting in the amphiphilic molecule C_{18}-PEG_6-4N1Ks (C18-PEG-Ks), which was performed under request by Covalab (Bron, France). C18-PEG-Ks was dissolved at a concentration of 20 mg/mL in a mixture of ethanol and water (EtOH 70%). Similar as for blank SNs preparation, VitE (200 mg/mL) and SM (40 mg/mL) and C18-PEG-Ks were mixed to obtain different mass ratios of the peptide (VitE:SM:C18-PEG-Ks

1:0.1:0.025–1:0.1:0.2, corresponding to a peptide concentration of 0.125–1 mg/mL) and ethanol was added to complete 100 μL. This organic phase was then injected into 1 mL of ultrapure water under continuous magnetic stirring for a couple of minutes. The formulations containing all the components were named SNs-Ks. A control formulation with only the VitE and the peptide was named V-Ks.

The association efficiency (AE%) of C18-PEG-Ks into the nanosystems was determined by direct quantification of the peptide using gradient HPLC analysis method. The isolation of nanosystems from free molecules was performed as follows: 1.5 mL of nanosystems (SNs-Ks, V-Ks) were injected into a dialysis cassette (Slide-A-Lyzer™ G2 Dialysis Cassette, Thermo Fisher Scientific, US) with a membrane molecular-weight cut-off (MWCO) of 20 KDa. Then the cassette was immersed in 800 mL of ultra-pure water with gentle stirring at room temperature (RT). The dialysis procedure was done for 2 h first then change water; another 2 h of dialysis and change water; then left for dialysis overnight. The new volume of nanosystems were measured after dialysis. Before injecting the nanosystems in HPLC column, they were dissolved in MetOH at a volume ratio of 1:20 (SNs:MetOH).

HPLC analysis was performed using a HPLC system 1260 Infinity II Agilent (Agilent Technologies, US) equipped with a pump G7111A, an autosampler G7129A, and an UV–Vis detector G7114A set at 220 nm wavelength. An InfinityLab Poroshell 120 EC-C18 (100 mm × 4.6 mm, 4 μm pore size) Agilent column was used and operated at RT. The mobile phases used were (A) ultrapure water with 0.1% (*v/v*) TFA, and (B) ACN with 0.1% (*v/v*) TFA The following gradient conditions were used; 0 min B = 20%; 1 min, B = 20%; 8 min B = 80%; 10 min B = 80%, 12 min B = 20%, maintaining a flow rate of 0.5 mL/min. Standard calibration curves were linear in the range of 7.8–250 ppm.

The association efficiency of C18-PEG-Ks into the nanosystems was calculated using the following equation:

Equation 1: Direct measurement of the encapsulated fraction.

$$AE\% = \left(\frac{Associated\mu g}{total\mu g}\right) \times 100$$

2.3. Physicochemical characterization of the nanosystems

Particle size and polydispersity index (PdI) of the nanoemulsions were determined by dynamic light scattering (DLS) after a dilution 1:20 (*v/v*) in water. The surface charge (Z-potential, ZP) values were obtained by Laser Doppler Anemometry (LDA) (Zetasizer NanoZS®, Malvern Instruments, Worcestershire, United Kingdom). Additionally, extended nanoemulsion characterization was performed by Nanoparticle Tracking Analysis (NTA) and Multiple-Angle Dynamic Light Scattering (MA-DLS). For NTA, the nanosystems were diluted at 1:1000 (*v/v*) in ultrapure water (NanoSight LM20, Amesbury, United Kingdom). Data collection was settled with 3 repeats/60 s capture time, with both shutter and gain manually determined for each sample. NTA 2.0 Build 127 software was used for measurement and subsequent data analysis. MA-DLS analyses were performed using an ALV SP − 86 goniometer with an ALV-5000 Multi-tau correlator and a Coherent Sapphire optically pumped semiconductor laser operating at λ = 488 nm and 200 mW power. Un-dialyzed samples were diluted 10 times with ultrapure water, while dialyzed samples were diluted 100 times. Measurements were performed at 25 °C and scattering angles between θ = 30° and 150° with increments of 10° and measuring times of 300 s. Results were analyzed using the ALV Correlator Software (ALV-5000/E version 3.0) based on the CONTIN algorithm adapted to the specific correlator noise. The logarithmically sampled relaxation time spectra (amplitude vs. log(τ)) were obtained from the CONTIN inversion of the normalised correlation functions. Assuming homodyne light beating, the distribution of diffusivities were obtained applying the relation $D = 1 / (q^2\tau)$, and transformed using the Stokes-Einstein relation, the solvent viscosity (η_0) and refractive index (n) at the actual temperature (T) in order to yield the hydrodynamic radius $R_H = kTq^2 / / 6\pi\eta_0$ where k is the Boltzmann constant, $q = (4\ \lambda\ n/\ \lambda)\ \sin(\theta/2)$ is the scattering vector as a function of wavelength in vacuum (λ), and scattering angle (θ).

The topography of the nanoemulsions systems was studied with Non-Contact Atomic Force Microscopy (NC-AFM) under ambient conditions. For this, AFM analysis samples were diluted with ultrapure water 100 times and 10 μL were deposited onto a mica substrate (SPI Supplies, Grade V − 1 Muscovite), allowed to dry and then viewed using a XE − 100 instrument (Park Systems, Korea) with a non-contact silicon cantilever probe with high resonant frequency (325 kHz) and backside aluminum reflex coating (ACTA, supplied by Park Systems).

2.4. Colloidal stability

The colloidal stability of the nanoemulsions was determined upon incubation with different medium as PBS 5 mM (1:2 *v/v*), cell culture medium RPMI (1:6 *v/v*) supplemented or not with 1% (*v/v*) FBS, and human serum previously filtered and diluted 10x in water (1:10, *v/v*), up to 24 h at 37 °C and under horizontal agitation (Bouzo et al., 2020; Mohr et al., 2014). The cell culture medium and plasma were tested under the same conditions without nanosystems, in order to ensure that the protein content of the media did not cause interferences. The colloidal stability of the nanosystems stored at 4 °C was also determined. Prior to DLS analysis, using Zetasizer NanoZS® (Malvern Instruments, Worcestershire, United Kingdom), all the samples (with or without media) were further diluted in ultrapure water at 1:10 (*v/v*).

2.5. In vitro toxicity

2.5.1. Metabolic activity assay

MCF7 breast cancer cells (ATCC, HTB-22) were seeded at a density of 1500 cells/well in 96-well plates and cultured in RPMI supplemented with 3% (*v/v*) FBS, at 37 °C in 5% CO_2 atmosphere. The next day, the cell culture medium was replaced by increasing concentrations of C18-PEG-Ks (0.25–50 μM) diluted in supplemented RPMI to a final volume of 150 μL per well. After 72 h of incubation with the nanosystems, the medium was aspirated and cells were washed with PBS 2x, and then 100 μL of MTT solution (5 mg/mL in PBS) were added to each well and incubated for 4 h. Afterwards, the formazan crystals were solubilized with 100 μL of DMSO and the absorbance was measured at 540 nm using a microplate reader (Multiskan EX, Thermo Labsystems). Cell viability (%) was calculated in percentage related to untreated (control) cells.

2.5.2. Colony forming assay (CFA)

MCF7 breast cancer cells were seeded in a 12-well plate at a density of 500 cells/well and cultured in RPMI supplemented with 10% (*v/v*) FBS, at 37 °C in 5% CO_2 atmosphere. After 24 h, cells were treated with increasing concentration of SNs-Ks and V-Ks (0.25 μM to 1 μM). SNs-blank and C18-PEG-Ks were used as positive controls. The cells remained in contact with treatment the whole period of the experiment, 10 days, which is the time needed for visible colonies to be formed. After this period, cells were incubated with MTT solution (5 mg/mL in PBS) for 4 h and subsequently dried and scanned. The obtained images were analyzed using ImageJ software (Rasband, n.d.).

2.5.3. Blood compatibility

Hemolysis assay was performed as follows, 100 μL of a 3% (*w/v*) suspension of heparin-stabilized erythrocytes were plated in a rounded bottom 96 well plate and incubated with the nanosystems (SNs-blank and SNs-Ks for 4 h at concentrations from 0.25 to 1 μM (added in a 50 μL total volume). Positive and negative controls were 50 μL /well of 1% Triton X-100 and PBS respectively. After incubation time, the plate was centrifuged at 1000 RPM for 10 min at 4 °C. Subsequently, 80 μL of the supernatant were transferred to another 96 well plate and read at 570 nm (absorption maxima of deoxyhemoglobin and oxyhemoglobin). Hemolysis percentage was calculated following the next equation.

Equation 2: Formula for calculation of the hemolysis percentage.

$$Hemolysis\% = \frac{Sample - PBScontrol}{TritonX100 - PBScontrol}$$

2.6. Cell uptake

The internalization of SNs, SNs-Ks was evaluated in MCF7 breast cancer cells by confocal laser scan microscopy (Leica microscope TCS SP8, Germany). Fluorescent SNs-blank and SNs-Ks were first prepared by supplementing a percentage of SM with the modified lipid TopFluor®-SM (5.6 μg/mL to achieve 25 ng/well of fluorescent matter). Cells were seeded in 8-well chamber slides 24 h before the experiment at a density of 50,000 cells/well and cultured in RPMI supplemented with 10% (*v/v*) FBS. The next day, cells were treated with fluorescently labeled nanosystems at a concentration of 0.5 μM (peptide) for 10 min, 30 min, 1 h, 2 h and 4 h. After the desired incubation time, cells were washed twice with PBS and fixed with paraformaldehyde (PFA) 4% (*w/v*) for 15 min at RT. Later, cellular nuclei were stained with Hoescht for 5 min and washed three times with PBS. Finally, the coverslips were mounted over the microscopy slides using Mowiol™ mounting medium (Calbiochem, UK), left to dry in darkness overnight and stored at −20 °C until visualization.

Furthermore, the internalization of SNs and SNs-Ks was also determined in MCF 7 cells by flow cytometry. In brief, cells were seeded in 6 well-plates at a density of 300,000 cells/well in RPMI supplemented with 10% (*v/v*) FBS. After 24 h, cells were treated with the fluorescently labelled nanosystems at a concentration of 0.5 μM (peptide) for 10 min, 30 min, 1 h, 2 h, and 4 h. Following these incubation times, cells were washed twice with PBS, and after trypsinization they were collected, resuspended and finally fixed in 500 μL of PFA 4% (*w/v*) for 15 min at RT. Samples were kept at 4 °C, protected from light, until flow cytometry analysis.

2.7. In vitro evaluation of SNs-Ks

2.7.1. Senescence escape assay

In order to determine the efficiency of SNs-Ks in preventing senescence escape and study their possible senolytic effects in chemotherapy-induced senescence model, a senescence escape assay was performed using MCF7 breast cancer cells. Cells were seeded in 6 well-plates at a density of 50,000 cells/well and cultured in RPMI supplemented with 3% (*v/v*) FBS, at 37 °C in 5% CO_2 atmosphere. After 24 h, cells were treated with doxorubicin at a concentration of 25 ng/mL for 96 h to generate MCF7 senescent cells (Guillon et al., 2019). After that, cell culture medium was aspirated, cells were washed with PBS and treated with the nanosystems for 24 h. Afterwards, the cells were washed with PBS and restimulated with fresh RPMI (10% *v/v* FBS) for 14 days. Emerged colonies were incubated with MTT solution (5 mg/mL in PBS) for 4 h and subsequently dried and scanned. Obtained images were analyzed using ImageJ software.

In order to make sure that after chemotherapy treatment (doxorubicin 25 ng/mL for 96 h) MCF7 cancer cell became senescent, the expression of cellular senescence markers such as β-galactosidase and p53/p21 were determined.

For β-galactosidase analysis, after doxorubicin treatment, the cells were fixed for 15 min at RT in 1% formaldehyde, then washed with PBS and incubated at 37 °C (in the absence of CO_2) with fresh staining solution (0.3 mg/mL of 5-bromo4-chloro-3 indolyl β-D-galactoside (X-Gal, Fermentas), 40 mM citric acid, 40 mM sodium phosphate at pH 6, 5 mM potassium ferrocyanide, 5 mM potassium ferricyanide, 150 mM NaCl, 150 mM $MgCl_2$ (all reagents were acquired from Sigma-Aldrich (Madrid, Spain)). SA-β-GAL-positive cells were quantified after 20 h.

The expression of p53 and p21 was assessed after 24 h of doxorubicin treatment, as p53 expression starts to decrease after this period. The expression of p21 and p53 was determined by western blot after protein extraction from the treated cells. The following antibodies were used: anti-p21Waf1 (Cell Signaling, 2947S), anti p-p53ser15 (Cell Signaling, 9284). Visualization was performed by chemiluminescence with a Bio-Rad Chemi Doc XRS imaging device (Bio-Rad) and Fusion Solo (Vilber).

2.8. Statistical analysis

All values were expressed as mean +/− standard deviation (SD). Differences were analyzed using non– parametric tests (*t* test, Mann–Whitney, Kolmogorov–Smirnov, and one-way ANOVA). Statistical analysis was performed using GraphPad Prism (Version 6.0 software) (GraphPad Software, San Diego, CA, USA). A p value < 0.05 was considered to be significant.

3. Results and discussion

Due to their specificity and potency, peptide drugs have accomplished a milestone with more than 80 products available on the market for different human conditions (cancer, diabetes, among others) and a serious investment ongoing. However, they still present limitations as short half-life and low bioavailability which limits their translation from the bench to the market (Bruno et al., 2013; Fosgerau and Hoffmann, 2015). Such issues can be improved by combining peptides with nanotechnology. Lipidic and polymeric nanocarriers have been described in the literature for protein and peptide delivery (Bruno et al., 2013; Chung, 2016; Fosgerau and Hoffmann, 2015). In the case of lipidic carriers, the peptide can be chemically conjugated to a hydrophobic chain thereby improving its encapsulation. In the case of the work herein described, this would not only enable the incorporation of the peptide into the nanosystems structure, but also to present the 4N1Ks peptide on the surface of the nanosystems to be available to interact with the respective receptor (CD47) expressed on the surface of the targeted senescent cells. The development of new strategies targeting senescent cells is of great relevance due to their role in age related diseases and cancer recurrence, thereby different pre-clinical and clinical studies are being conducted to address this avenue to further understand and fight such diseases.

3.1. Development and characterization of SNs-Ks

In order to incorporate 4N1Ks peptide into SNs structure and potentiate its presentation on their surface, our strategy was to chemically conjugate the peptide to a PEGylated stearic acid carbon chain (C18). PEGylated lipids have been used as a base to conjugate biomolecules like peptides and antibodies to the surface of nanoformulations (Bouzo et al., 2021). In addition, PEG has been extensively used in drug delivery formulation as it prolongs blood circulation time and reduces possible interactions with blood components like proteins (opsonisation), providing 'stealth' properties to nanosystems (Berrecoso et al., 2020).

In this work, the nanosystems were prepared by the single-step ethanol injection method, where the modified peptide was mixed with the other organic phase components and injected in ultra-pure water and these were named SNs-Ks. We hypothesized, that through the formulation process the modified peptide would rearrange itself so the hydrophobic part (stearic acid chain) would be incorporated in the oil core while the PEG-Ks part would be exposed on the surface of the nanosystems, as illustrated in Fig. 1. In this way the PEG moiety could also improve the nanosystems colloidal stability. In fact, due to the new structure, the modified peptide might work as a surfactant and promote the disposition of the peptide on the surface of the nanosystems. In order to address this hypothesis, we decided to formulate simply with VitE and C18-PEG-Ks (V-Ks). In this way we could determine if in the absence of sphingomyelin, the modified peptide in combination with VitE would be able to form nanostructures as SM is able to. Thereby, in this work V-Ks nanosystems were simply used as controls in order to provide evidence regarding the capacity of the modified peptide to emulsify and its arrangement on the nanosystems structure.

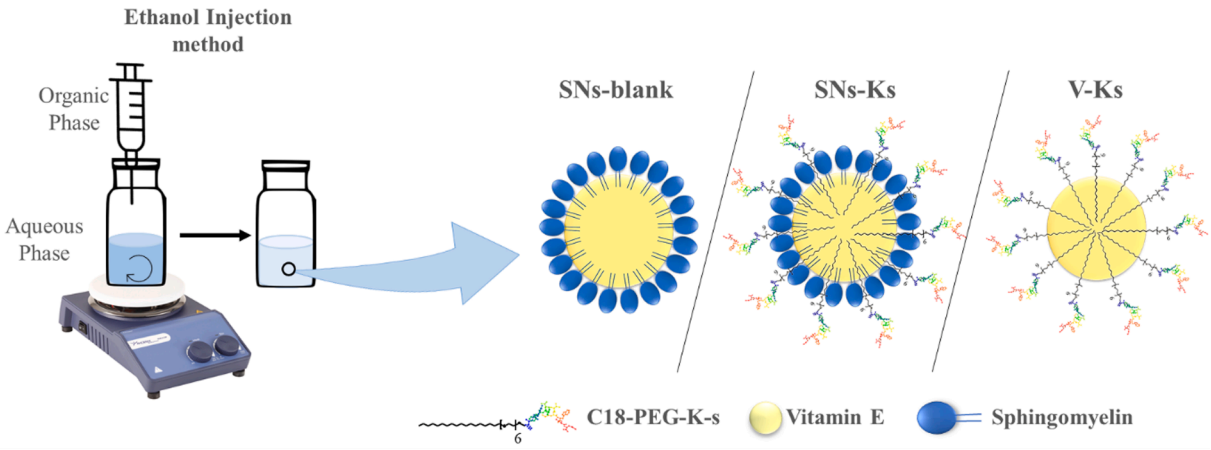

Fig. 1. Schematic illustration of the nanosystems (SNs-blank, SNs-Ks and V-Ks) preparation by ethanol injection method.

Based on a previous study from our group, showing the great colloidal stability under accelerated storage conditions of the VitE:SM at 1:0.1 ratio, with around 100 nm of size and slightly negative zeta potential, this ratio was selected for the present work (Bouzo et al., 2020). As shown in Fig. 2 (upper panel), the incorporation of the peptide at the weight ratios 0.025, 0.05 and 0.1 (respective to VitE) did not

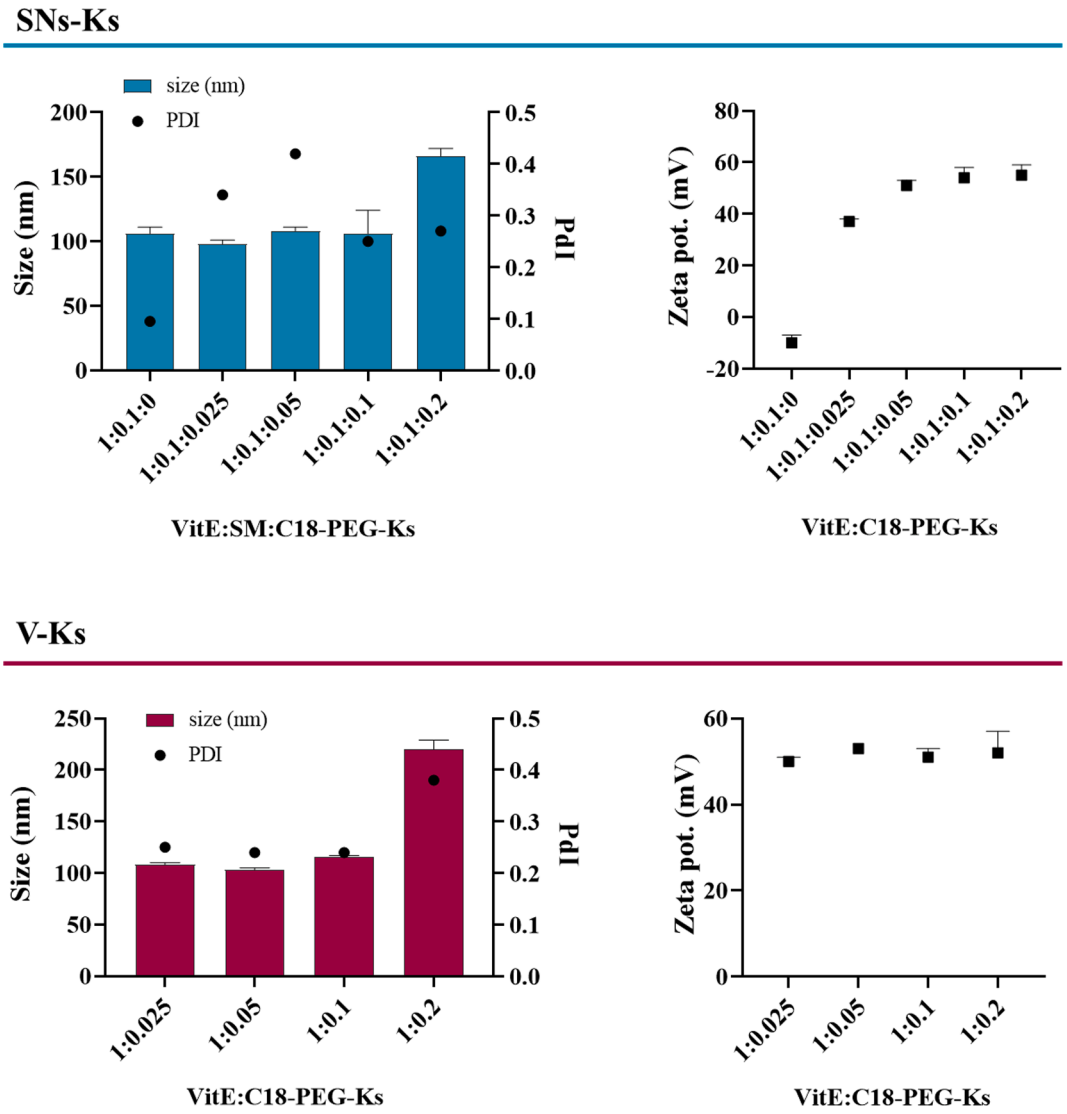

Fig. 2. Effect of increasing weight ratios of C18-PEG-Ks (from 0.0025 to 0.2, respective to VitE) on SNs-Ks' (composed of VitE, SM and C18-PEG-Ks) and V-Ks' (composed of VitE and) size, polydispersity index (PdI) and zeta potential, determined by DLS.

significantly alter the hydrodynamic diameter of the nanosystems, however doubling the ratio of the peptide to 0.2 led to an increase of the size from 106 to 167 nm. Regarding the control V-Ks, C18-PEG-Ks ratios ranging from 0.025 to 0.1 resulted in the formation of nanostructures with a hydrodynamic diameter below 120 nm (Fig. 2), similar to SNs-blank (1:0.1:0) and SNs-Ks (1:0.1:0.025–1:0.1:0.1). As observed for SNs-Ks, increasing the ratio of the modified peptide to 0.2 resulted in a bigger size of 220 nm but also to less homogeneous population as indicated by the bigger PdI (0.38). This can be explained due to the surfactant-like characteristics of the peptide conjugated to a PEGylated hydrophobic chain that, as reported in several studies, increasing amounts of surfactants lead to a smaller size of the oil droplets, however when exceeding a specific concentration lead to an increase in the particle size and can also result in unstable nanosystems (Kommuru et al., 2001; Saberi et al., 2013; Wang et al., 2009). In addition, unlike SNs-blank (−10 mV) both SNs-Ks and V-Ks presented a positive zeta potential (+50 mV) which was expected due to the 4N1Ks peptide's positively charged amino acids (lysin and arginine). Both the capacity of C18-PEG-Ks to form nanostructures with VitE and the positive surface charge of SNs-Ks and V-Ks provide evidence regarding the peptide surfactant properties and its availability on the nanosystems surface.

In order to further characterize the physicochemical properties of SNs-Ks at 1:0.1:0.1 (VitE:SM:C18-PEG-Ks, w/w), other methods namely NTA, MA-DLS and AFM were used. SNS-blank (1:0.1, VitE:SM) and V-Ks (1:0.1, VitE:C18-PEG-Ks) were used as controls. The nanosystems loading C18-PEG-Ks at the ratio 0.1 were selected for further characterization considering their size (about 100 nm) as well as population homogeneity (PdI < 0.3) and 4N1Ks peptide senolytic effective dose (50 μM).

As shown in Fig. 3 these nanosystems were dialyzed and characterized once again by DLS (before and after dialysis) in order to understand if this mild process could impair SNs-Ks physicochemical properties. This method was selected to isolate the nanosystems from the free C18-PEG-Ks molecules, as well as to determine the association efficiency of the peptide. DLS analysis showed that neither particle size or PdI (Fig. 3) nor surface charge (data not shown) were affected during the dialysis process. In addition, two weeks after dialysis, DLS analysis was repeated without showing significant changes in size, PdI nor zeta potential (data not shown). The nanosystems were also characterized by NTA and MA-DLS before and after dialysis, as complementary methods of DLS. NTA combines laser light scattering microscopy with a charge-coupled device camera and therefore grants identifying and tracking individual nanoparticles moving under Brownian motion, determining particle size and calculating particle concentration (Filipe et al., 2010). NTA data (Table 1) shows that dialyzed nanosystems presented a slightly smaller mean particle size as well as span value, which indicates a smaller size distribution and a more homogenous sample. The dialyzed nanosystems homogeneity is also observed in Fig. 3 (lower panel). This probably indicates that the SM and modified peptide free molecules were exchanged through dialysis. D-values D10, D50, and D90, are representative of the particle diameter at 10, 50 and 90% cumulative distribution (Table 1). In general, these results are compatible with the DLS data.

The second complementary method selected for the characterization of the nanosystems' physicochemical properties was MA-DLS. A single relaxation mode was observed. This mode is angular-dependent, as expected for translational Brownian diffusion of the nanosystems. Linearly-fitting the angular dependence of the inverse relaxation times for these diffusion modes (τ^{-1} vs. q^2), we obtain an average diffusion coefficient of the nanosystems. The analysis revealed the existence of a single and clear relaxation mode for blank SNs, SNs-Ks and V-Ks in the whole scattering range. For SNs-blank and SNs-Ks sample, the average diffusion coefficients determined were 4.454 ± 0.006 and $\mu m^2/s$ and 5.476 ± 0.017 $\mu m^2/s$, which correspond to an average hydrodynamic

Table 1
Physicochemical properties of SNs-blank (1:0.1), SNs-Ks (1:0.1:0.1) and V-Ks (1:0.1) before and after dialysis, determined by NTA. Mean particle size (diameter), D-values (D10, D50, D90), calculated SPAN value and sample concentration in particles per milliliter (particle/mL) (mean ± SD, n = 3).

Nanosystems	Mean size (nm)	D10	D50	D90	Span	Concentration (particles/mL)
SNs-blank	122 ± 1	93 ± 1	113 ± 1	166 ± 3	0.64	$1.8 \times 10^{12} \pm 2.5 \times 10^{10}$
SNs-blank dialyzed	123 ± 1	96 ± 1	116 ± 1	155 ± 3	0.50	$5.1 \times 10^{11} \pm 9.6 \times 10^{9}$
SNs-Ks	108 ± 27	76 ± 18	96 ± 26	159 ± 34	0.87	$3.7 \times 10^{11} \pm 1.9 \times 10^{10}$
SNs-Ks dialyzed	74 ± 19	58.8 ± 1	69 ± 1	98 ± 6	0.57	$2.8 \times 10^{11} \pm 2.6 \times 10^{10}$
V-Ks	111 ± 32	81 ± 15	101 ± 30	152 ± 52	0.67	$4.3 \times 10^{11} \pm 2.8 \times 10^{10}$
V-Ks dialyzed	90 ± 3	69 ± 2	84 ± 1	121 ± 13	0.54	$6.5 \times 10^{11} \pm 6.3 \times 10^{10}$

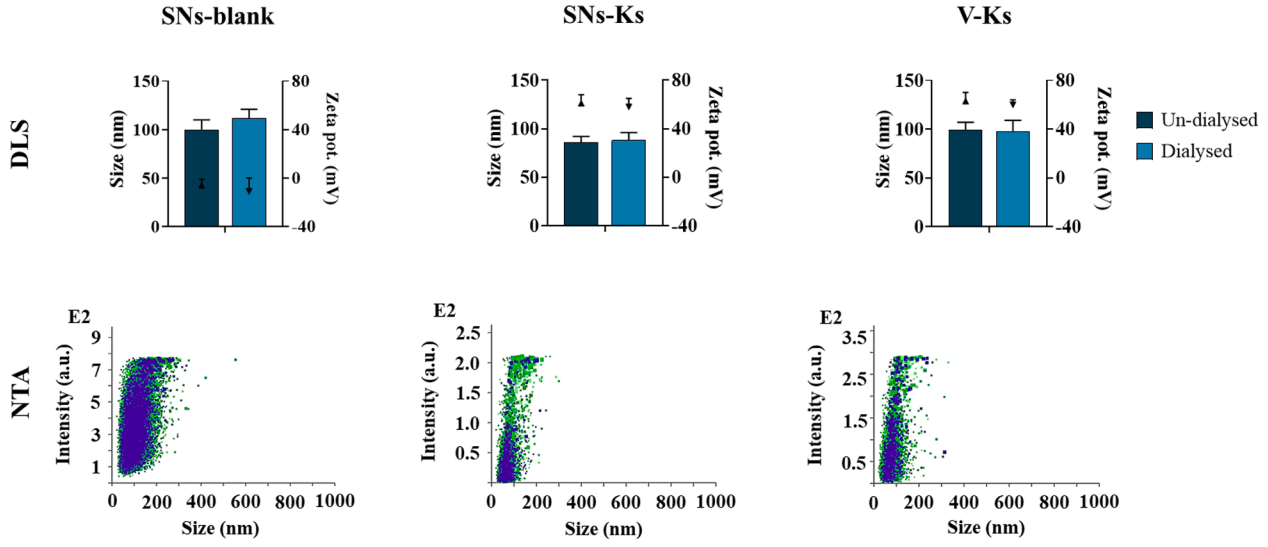

Fig. 3. Physiochemical characterization of dialyzed vs un-dialyzed SNs-blank (left), SNs-Ks (middle), and V-Ks (right) nanosystems by Dynamic light scattering (DLS) and dialyzed nanosystems by Nanoparticle tracking analysis (NTA) (n ≥ 3).

radius of about 55.04 ± 0.08 and 44.76 ± 0.14 nm, respectively. And finally, for the V-Ks sample, the average diffusion coefficient was 5.564 ± 0.007 $\mu m^2/s$, which corresponds to an average hydrodynamic radius of $R_H \approx 44.06 \pm 0.06$ nm. In addition, Fig. 4 shows that these nanosystems have a main population (R_H between 40 and 60 nm, as previously determined) and a reduced presence of a subpopulation with smaller size, which was only possible to observe due to the measurements performed with different scattering angles. The average results summarized in Table 2, in general, are very consistent with the ones observed by both DLS (Fig. 3) and NTA (Fig. 3 and Table 1) analysis, showing the reproducibility of the formulations and their suitability to be characterized by different techniques.

Atomic force microscopy was also explored in order to check the heterogeneity of the particle population. Regarding this technique, only the dialyzed samples were analyzed because the un-dialyzed ones showed a bed of material deposited on the mica surface caused by the different components of the nanosystems that probably were solubilized outside the nanoemulsion. The AFM images were acquired immediately after deposition of the samples on the mica surface, showing clearly the characteristic spherical shape of the SNs (Fig. 5), previously observed in other works through TEM analysis (Bouzo et al., 2020). This spherical shape did not seem to be affected by the incorporation of the modified peptide. As shown in Table 2, in most of the depositions, the average peak-to-valley distance (R_{pv}), obtained for the nanoemulsions are below the expected sizes observed in solution. This was an expected result because the nanoemulsion droplets are spread on the mica surface after deposition and drying. The AFM heights observed for the nanoemulsion droplets of SNs and SNs-Ks did not show a clear decrease in height with time (at least during several hours), pointing out the good stability of these nanosystems. Regarding V-Ks a phase segregation of some components was observed with time, finally resulting in the coalescence of several nanoemulsion droplets (Fig. 5, bottom right). This evolution over time was also observed by B. Ruozi et al. (Ruozi et al., 2005). This control formulation also led us to understand that the modified peptide has the capacity to behave as a surfactant due to its amphiphilic structure, and that it requires the presence of another component as sphingomyelin to form stable nanosystems, as it is the case of SNs-Ks.

Regarding the AE of the modified peptide to SNs-Ks (1:0.1:0.1), determined by HPLC after dialysis, the results showed a high AE of 87.2 ± 6.9%, which correlates with a loading capacity (LC%) of 7.3% for SNs-Ks (1:0.1:0.1). The control formulation V-Ks (1:0.1) also presented a similar AE (90.3 ± 10.6%), which once again indicates that C18-PEG-Ks is acting as a surfactant being able to emulsify with VitE (and SM) and form nanostructures. Note that in order to ensure that none of the nanosystems components affected the HPLC signal of the peptide, mixtures of Vit E/C18-PEG-Ks and SM/C18-PEG-Ks were also analyzed. In addition, a dialysis control using only C18-PEG-Ks was also performed, showing that about 80% passed through the membrane.

Table 2
Physicochemical characterization of nanosystems (before and after dialysis) by MA-DLS and AFM.

Nanosystems	Average Diffusion Coefficient, D ($\mu m^2/s$)	Average Hydrodynamic Radius, R_H (nm)	Average Peak-to-Valley distance, R_{pv} (nm)
SNs-Blank	4.454 ± 0.006	55.04 ± 0.08	–
SNs-Blank dialyzed	5.108 ± 0.018	47.99 ± 0.17	51.2 ± 29.6
SNs-Ks	5.476 ± 0.017	44.76 ± 0.14	–
SNs-Ks dialyzed	6.598 ± 0.004	37.17 ± 0.02	22.0 ± 11.2
V-Ks	5.564 ± 0.007	44.06 ± 0.06	–
V-Ks dialyzed	5.569 ± 0.007	44.02 ± 0.06	88.1 ± 29.7

As verified by DLS, NTA, MALS, AFM and HPLC quantification, the modified peptide was efficiently incorporated in SNs structure. Therefore, as initially hypothesized, the chemical conjugation of the 4N1Ks peptide to PEGylated carbon chain (stearic acid, C18) provided an amphiphilic character to the peptide, and therefore surfactant-like properties. Nonetheless, AFM data showed that despite being able to form nanostructures with Vit E, these are not stable and require the presence of another surfactant, in this case sphingomyelin. In addition, this extensive characterization before and after dialysis is of extreme importance in order to guarantee that the formulation maintains its features and can be used either in an *in vitro* or *in vivo* scenario.

3.2. SNs-Ks stability over time and in biorelevant media

Evaluating the stability of prepared nanosystems overtime and in different biological media is essential to predict the fate of nanosystems especially after administration (Wu et al., 2011). Storage stability at 4 °C was studied and the analysis by DLS showed that SNs-Ks (103 ± 17 nm, PdI 0.2, +51 ± 9 mV) and V-Ks (112 ± 14, PdI 0.2, +51 ± 3 mV) were stable at least for 6 months. Similar results were observed upon storage of the nanosystems at RT, for at least 3 months (SNs-Ks, 119 ± 1 nm, PdI 0.2, +51 ± 1 mV and V-Ks, 129 ± 1, PdI 0.1, +54 ± 0 mV). In addition, the stability of SNs (with and without the modified peptide) was determined in different biological media, PBS 5 mM, RPMI (supplemented or not with 1% FBS) and human plasma. According to DLS measurements and optical visualization of the samples after incubation

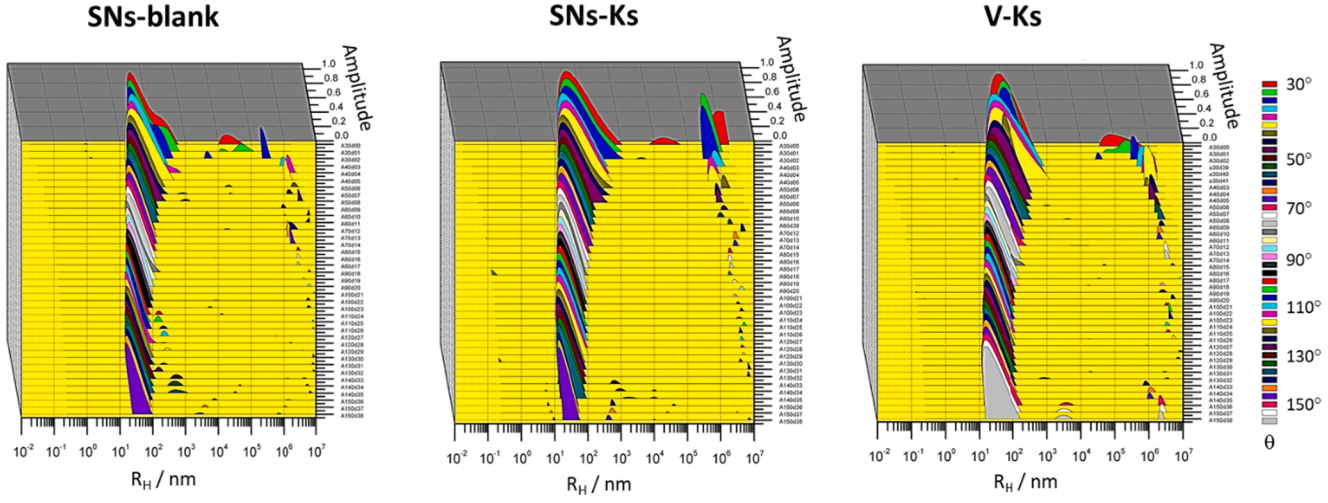

Fig. 4. Physicochemical characterization of dialyzed nanosystems by Multi angle dynamic light scattering (MA-DLS) (n = 3). 3D plots show CONTIN-derived hydrodynamic radii distributions for different scattering angles (θfrom 30–150°).

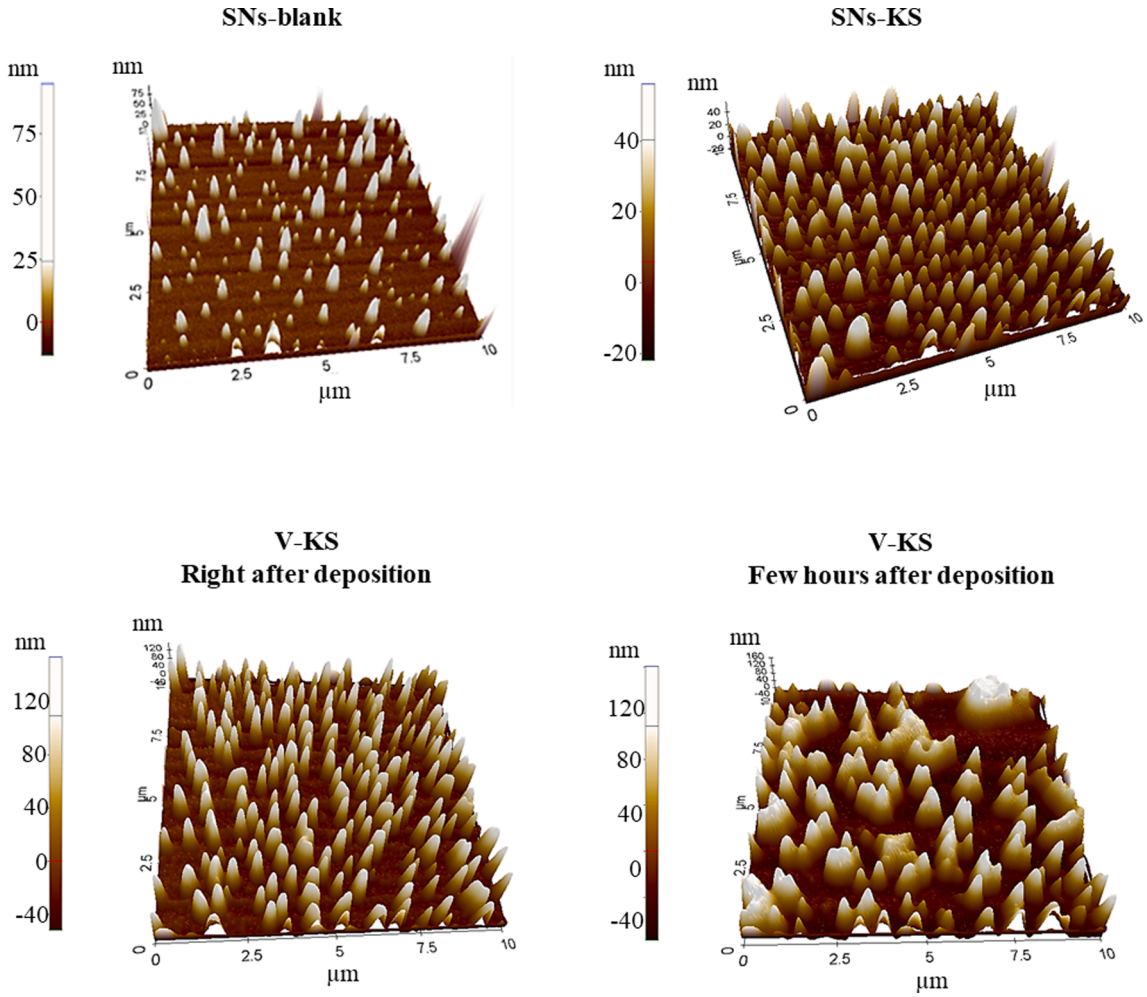

Fig. 5. Physiochemical characterization of dialyzed nanosystems by Atomic force microscopy (AFM) (n = 3).

with the different media, it was possible to observe that SNs-Ks (1:0.1:0.1) was stable in the cell culture medium containing proteins (FBS). This could be related to the adsorption of serum proteins to the surface of the strongly positively charged SNs-Ks nanosystems, through electrostatic interactions which can also explain the increase in size to 272 ± 10 nm and surface charge decrease to −11 ± 1 mV, after 24 h of incubation in RPMI supplemented with 1% FBS. Based on the possibility that a lower content of modified peptide could result in better colloidal stability due to a lower positive surface charge of the nanosystems, the colloidal stability of SNs-Ks prepared at 1:0.1:0.025 ratio was also assessed in supplemented RMPI. However, this nanosystem was only stable in RPMI supplemented with 1% FBS showing a final hydrodynamic size of 206 ± 7 nm (after 24 h incubation), which was a smaller increment in comparison to 1:0.1:0.1 SNs-Ks. Such behavior is reported for other positively charged nanosystems (Aramesh et al., 2015). On the other hand, the colloidal stability in plasma gives an indication of the nanosystems' fate after intravenous (IV) administration. The plasma was diluted 10 times in ultra-pure water before mixing it with the prepared nanosystems, so that the plasma contents did not interfere with the DLS. As it is clear from Fig. 6, SNs-blank and SNs-Ks nanosystems were both stable in plasma for 24 h presenting a mean particle size of 101 ± 11 nm and 149 ± 3 nm for SNs-Ks and SNs-blank, respectively, at the end of the experiment.

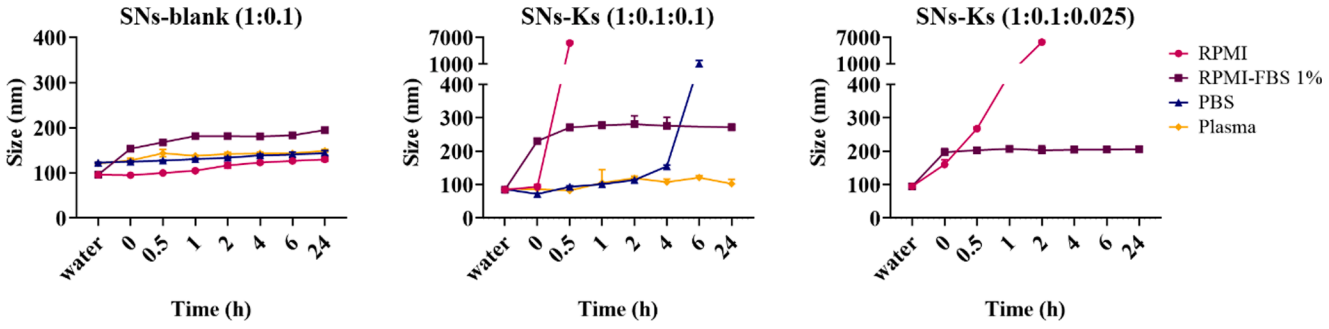

Fig. 6. Stability of SNs-blank (1:0.1) and SNs-Ks (1:0.1:0.1 and 1:0.1:0.025) upon incubation in different relevant media (PBS 5 mM, non-supplemented RPMI, RPMI supplemented with 1% FBS and plasma) up to 24 h. PBS: Phosphate Buffer Saline; FBS: Fetal Bovine Serum.

3.3. In vitro evaluation of the nanosystems

3.3.1. SNs-Ks effects on MCF7 and red blood cells

Assessing the cytotoxic profile of the nanosystems is an important requirement for newly formulated therapeutic nanosystems (Fornaguera and Solans, 2017), since it provides an estimation of possible undesired side effects. The toxicity profile of the nanosystems containing the peptide (SNs-Ks and V-Ks) in comparison with SNs-blank was assessed through proliferation studies namely cells' colony forming and metabolic activity, as well as hemolytic assay.

Essentially, colony forming assay is the method of choice to determine cell reproductive death after treatment (ionizing radiation, genetic manipulation, etc.) as well as the effectiveness of cytotoxic drugs (Franken et al., 2006). It determines the ability of a single cell in the population, undergoing treatment, to grow into a colony of at least 50 cells by clonal expansion. To make sure that the chemical modification did not alter its efficacy C18-PEG-Ks cytotoxicity as well as capacity to impair the formation of tumoral cells colonies were assessed by MTT and colony forming assays MCF7 cells were treated with a range of C18-PEG-Ks concentrations (1–50 μM). Regarding cell viability assays, cells were treated for 72 h, while in the case of CFA, cells were treated for 24 h and left in culture in cell culture medium for another 10 days (period required to observe the formation of colonies). Fig. 7A shows that C18-PEG-Ks maintained its dose-dependent cytotoxic profile which at 50 μM led to about 90% mortality of MCF7 cells. On the other hand, its anti-proliferative capacity and thereby impairment of colonies formation was also not affected since the wells treated with 15–50 μM were totally clear, while at 5 μM MCF7 cells capacity to form colonies was only decreased by 50% (Fig. 7 B and C). The C18-PEG-Ks cytotoxic profile is similar to 4N1Ks peptide, as previously observed (Jatal et al., 2021), indicating that C18-PEG modification did not alter 4N1Ks efficacy.

Considering that we expected an improved efficacy by formulating the modified peptide into a nanosystem, we decided to continue the study using C18-PEG-Ks concentrations below 5 μM. In addition, before studying the cytotoxicity of the nanosystems containing the peptide, it was important to determine if the SNs-blank did not cause any toxic effects at the concentrations of interest. According to the results presented in Fig. 7D, the SNs-blank were toxic at 1 μM while no apparent toxicity was observed at 0.5 μM compared to not-treated wells. Therefore, the effect of SNs-Ks was assessed from 0.25 up to 1 μM. Interestingly, at 0.5 μM SNs-Ks were able to significantly decrease ($p < 0.01$) the proliferative capacity of MCF7 cells by almost 50% in comparison to non-treated cells (Fig. 7E). Decreasing the effective concentration 10 times (from 5 to 0.5 μM) is quite remarkable and could be attributed to the association of 4N1Ks peptide to the nanosystems and its exposure on their surface. Such results demonstrate the capacity of the nano-formulated systems to improve drug's effectiveness, thereby requiring lower doses.

The nanosystems' surface charge, concentration, shape and size can also be responsible for toxic effects on red blood cells once administered IV (de la Harpe et al., 2019). Thereby, hemocompatibility is a crucial requirement for any newly formulated therapeutic nanosystem intended to be delivered intravenously. For that, we assessed the blood compatibility of SNs-Ks (1:0.1:0.1) in comparison with SNs-blank nanosystems. The results presented in Fig. 7F, indicate that while triton caused RBCs' hemolysis, SNs-blank did not affect RBCs integrity (as previously reported by our group (Bouzo, 2019)) while the SNs-Ks presented a moderate haemolytic effect up to 5 μM (Weber et al., 2018), that could be due to their positive surface charge. Still, according to other works, all the tested SNs-Ks concentrations are within an acceptable range of haemolysis (5–25%) (Dobrovolskaia et al., 2008). Thereby, we continued with the *in vitro* characterization of the nanosystems.

3.3.2. Internalization by MCF7 cells

In order to elucidate the effect of 4N1Ks peptide association to the surface of SNs nanosystems on cellular uptake, SNs-Ks with fluorescently

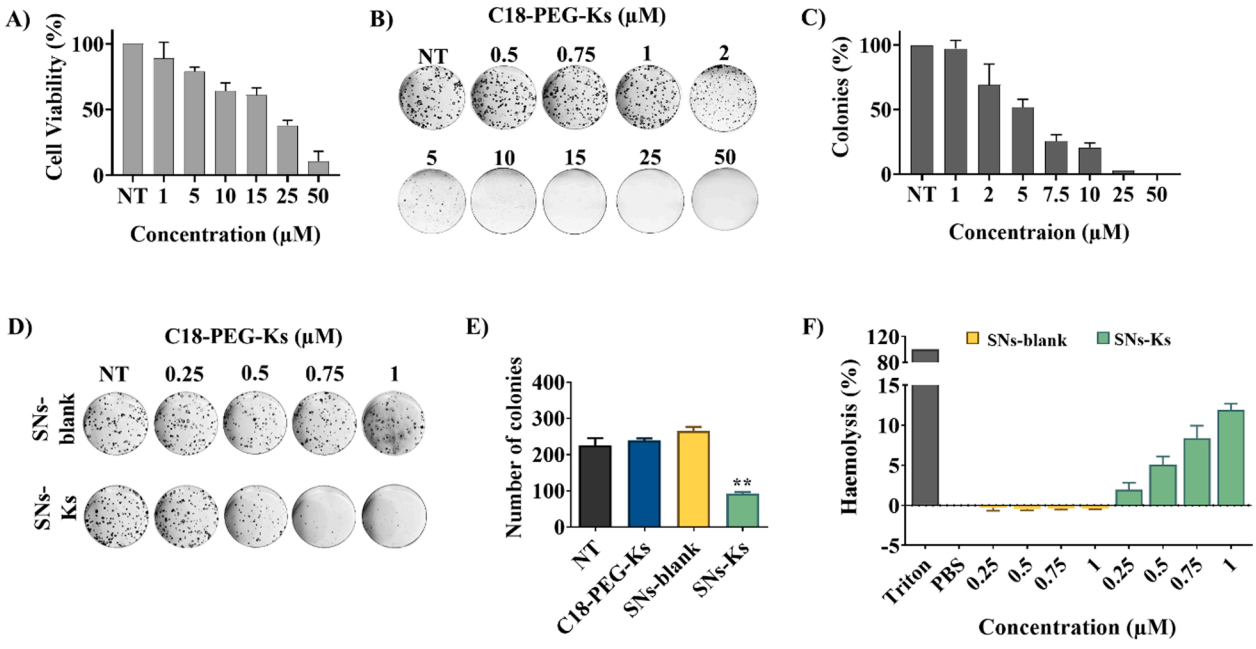

Fig. 7. Effect of C18-PEG-Ks and SNs-Ks on MCF7 breast cancer cells and red blood cells. A) MCF7 cells viability determined by MTT assay after treatment with the modified peptide (1–50 μM) for 72 h. B) Macroscopic photos of MCF7 colonies formed after C18-PEG-Ks treatment. C) Evaluation of cell proliferation activity by colony forming assay of MCF7 treated with C18-PEG-Ks (1–50 μM) for 10 days. D) Representative macroscopic images of MCF7 colonies. MCF7 cells after treatment for 9 days with C18-PEG-Ks, SNs-blank and SNs-Ks (peptide concentration 0.25–1 μM). E) Graphical representation of MCF7 colony forming capacity upon treatment with cell culture medium (NT, non-treated), C18-PEG-Ks, SNs-blank and SNs-Ks at 0.5 μM (peptide concentration). Data are presented as mean ± SD (n = 6). ** $p <$ 0.01. F) Human red blood cells were hemolysis (%) upon exposure to SNs-blank and SNs-Ks nanosystems up to 1 μM (peptide). Triton X-100 and PBS were used as positive and negative controls representing 100% and 0% of hemolysis, respectively (n = 3). Data are presented as mean ± SD. (For interpretation of the references to colour in this figure legend, the reader is referred to the web version of this article.)

labeled sphingomyelin were prepared and internalization studies in MCF7 cells was assessed by confocal microscopy and flow cytometry. Confocal microscopy images illustrated in Fig. 8, show an early detection of SNs-Ks (1:0.1:0.1) in and around MCF7 cells after 30 min of treatment and the highest fluorescent signal was detected 2 h after treatment. On the other hand, the highest fluorescent signal for SNs-blank was only detected 4 h after treatment. Similarly, and more interesting observations were found by flow cytometry analysis, which indicated that about 83% of MCF7 cells were fluorescent after only 10 min of treatment with SNs-Ks nanosystems reaching 96% after 1 h of treatment. In the case of SNs-blank, a similar percentage of fluorescent MCF7 cells was only achieved 2 h after treatment. These results can be explained by i) the positive surface charge of SNs-Ks can play a role in the enhanced cellular uptake through electrostatic interactions with the negatively charged cells' membrane (Forest et al., 2015); ii) several papers point out that the presence of conjugated ligands on nanoparticles improve cellular uptake (Fakhari et al., 2011; Gao et al., 2013); iii) most importantly, 4N1Ks peptide target is CD47 receptor which is expressed on the surface of MCF7 breast cancer cells as well as of senescent cells which could improve cell uptake of SNs-Ks nanosystems.

3.3.3. Senescence escape

After assessing the capacity of SNs-Ks to i) efficiently associate the modified peptide, ii) improve SNs internalization in cells, iii) potentiate 4N1Ks peptide effect on decreasing MCF7 colony forming capacity while iv) showing a reduced hemolytic effect on RBCs, the last and most important study in this work was to determine if SNs-Ks nanosystems improved the senolytic effect of 4N1Ks peptide.

Senescent cells were initially considered to be involved in tumor suppressor mechanisms for being in cell cycle arrest, as well as for the senescent-associated secretory phenotypes (SASPs) which secretes cytokines, chemokines, among other molecules, that attract different immune cells responsible for the elimination of anomalous cells (cancerous, senescent…). Nonetheless, cellular senescence is a highly dynamic and heterogeneous state and thereby the accumulation of these cells and due to SASP activity they can also be harmful behaving as protumorigenic through different mechanisms. Several anticancer therapeutics (chemotherapy, radiotherapy, among others) have been recognized to induce cellular senescence either in tumoral and healthy cells. However, the tumoral cells that can escape senescence state end up being more aggressive with higher proliferation rates (Acosta and Gil, 2012; Milanovic et al., 2018; Yang et al., 2017).

SNs-Ks senolytic activity was assessed using a chemotherapy-induced model of MCF7 cells. For that, first senescent MCF7 cells were generated upon the treatment with doxorubicin (25 ng/mL for 4 days). The senescence-like phenotype of MCF7 cells was displayed by their changed morphology (larger size, flattened shape, cytoplasmic granularity), increased β-galactosidase activity as well as increased expression of senescence marker p21 (Fig. 9A). The senescent cells were treated with SNs-Ks and SNs-blank (as control) for 24 h. The treated cells were left for 14 more days in cell culture medium, in order to observe the establishment of macroscopic colonies. In this way we could determine if SNs-Ks were able to deplete the senescent cells and therefore avoid or decrease their capacity to escape senescent state. If the cells can recover their proliferative state after being senescent, they would not only be able to form colonies, as we assessed in this study, but also to become more aggressive, as shown in other studies (Milanovic et al., 2018; Yang et al., 2017).

Despite the extensive research on cellular senescence, therapeutic drugs aiming to impair their pro-tumorigenic effects and the several benefits of nanotechnology, only a few studies have combined these drugs with a nanocarrier. In addition, such studies have been mainly focused on the use of inorganic nanoparticles (mesoporous, metallic, calcium carbonate NPs) mainly targeting senescent cells based on their high β-galactosidase activity (Agostini et al., 2012; Muñoz-Espín et al., 2018) but also making use of quercetin (Lewinska et al., 2020) and CD9 monoclonal antibody (Thapa et al., 2017). More recently, Belcastro et al developed maleimide-decorated Labrafac nanoemulsions for the grafting of anti-VCAM-1 antibody, aiming at the targeting of endothelial senescent cells (Belcastro et al., 2021). Aside from being developed as a therapeutic approach, when loading lipophilic fluorescent dyes, these nanosystems can also be considered for diagnosis.

Unlike these nanosystems, in the present work we used natural components as Vitamin E and sphingomyelin for the main composition, formulated using the single-step ethanol injection method, which is highly reproducible, simple and straightforward. For senescent cells targeting, we selected peptide 4N1Ks which is derived from the C-terminal domain of TSP-1, that targets CD47 receptor (Guillon et al., 2019), and has the ability to prevent senescent cells escape by promoting autophagy in senescent and cancer cells (Jatal et al., 2021). The results presented in Fig. 9B-C show that SNs-Ks significantly reduced the number of emergent colonies in comparison to non-treated as well as SNs-blank treated cells, specially at 0.5 μM (peptide). A similar effect on colony forming capacity was also observed on cancer MCF7 cells' CFA. Considering the results, these nanosystems might present a viable approach for reducing the burden of accumulated senescent cells caused due to anticancer treatments as chemotherapeutics, and therefore make a step forward in the management of this disease. Still, further *in vivo*

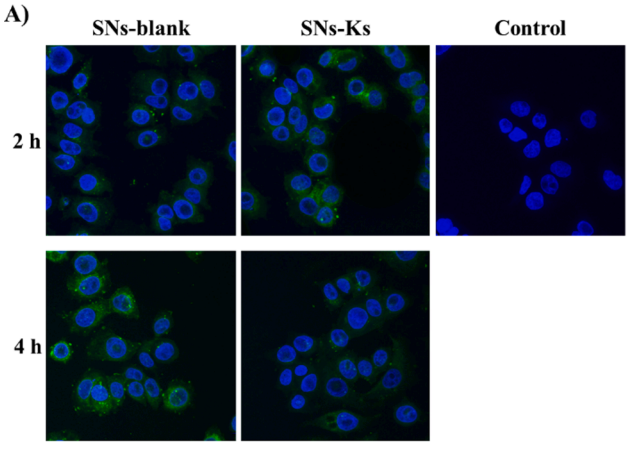

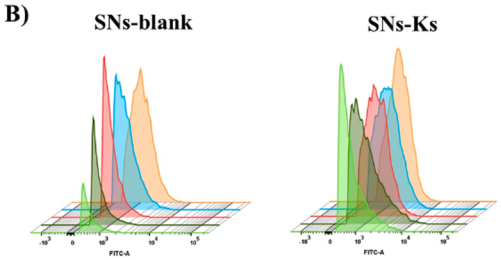

	TopFluor-Positive cells (%)				
	10 min	30 min	1 h	2 h	4 h
SNs-blank	22	50	81	93	99
SNs-Ks	83	92	96	97	99

Fig. 8. Cell internalization studies of SNs-Ks and SNs-blank over time. (A) Confocal microscopy images of the internalization of SNs-Ks and SNs-blank, labelled with TopFluor®-SM,in MCF7 cells after 30 min, 1 h and 2 h of treatment. Green channel: TopFluor®-SM labelled SNs. Blue channel: nuclei staining with DAPI. (B) Flow cytometry analysis and respective percentage of MCF7 cells internalizing TopFluor-SM SNs over time (10 min to 4 h). (For interpretation of the references to colour in this figure legend, the reader is referred to the web version of this article.)

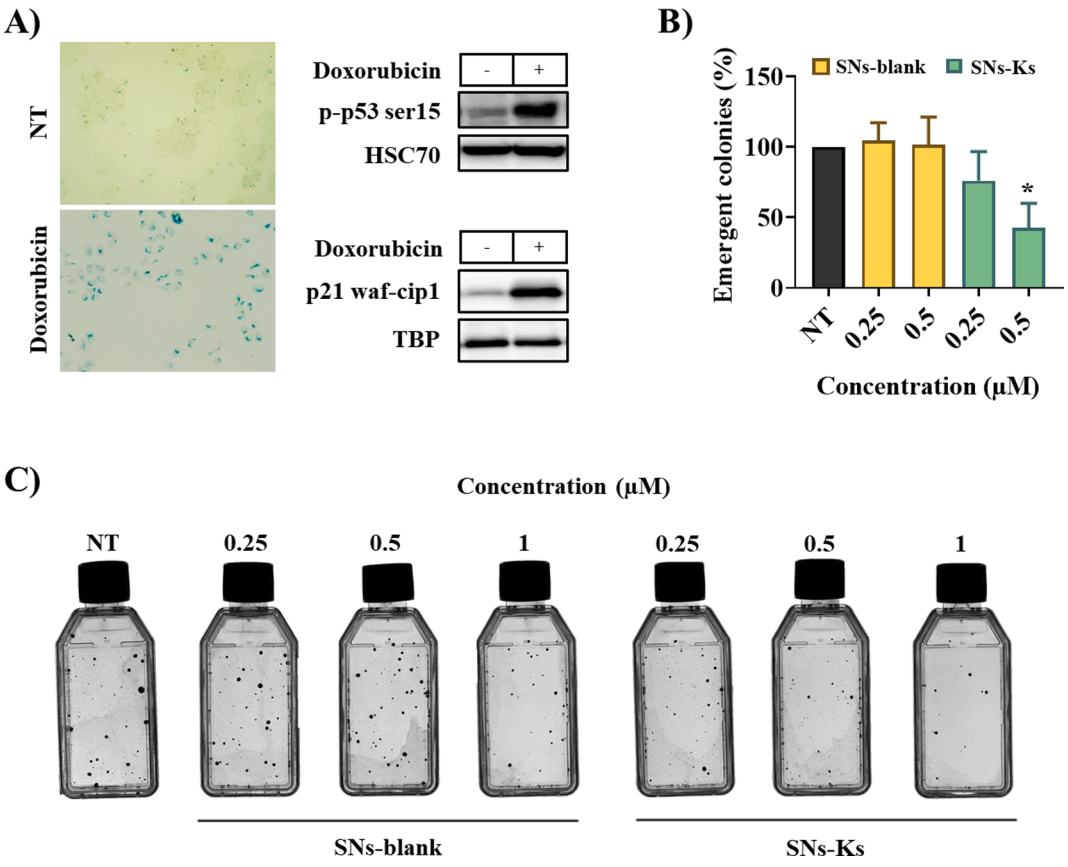

Fig. 9. SNs-Ks effect on senescence escape. A) Microscopic photos of β-galactosidase staining show that MCF7 breast cancer cells became senescent upon the treatment with doxorubicin (25 ng/mL for 96 h) when compared to non-treated (NT) cells. Doxorubicin-induced senescence of MCF7 cells was also demonstrated by the expression of senescence markers p-p53 ser15 and p21 waf-cip1, determined by western blot after 24 h treatment. B) Graphical representation of SNs-Ks' effect on the capacity of senescent MCF7 cells colonies to emerge and proliferate again. The senescent cells were treated with 0.25 and 0.5 μM (peptide dose) of SNs-Ks and SNs-blank for 24 h and left for more 14 days in cell culture medium. Non-treated (NT) cells and SNs-blank were used as positive and negative controls, respectively (n = 4). *p < 0.05. C) Macroscopic images of senescent MCF7 cells colonies after treatment with SNs-Ks and SNs-blank at increasing concentrations (0.25–1 μM, referring to the peptide concentration).

studies will be needed to confirm the therapeutic potential.

4. Conclusions

In this study we successfully prepared promising Vitamin E-sphingomyelin nanosystems, through the very simple and efficient method of ethanol injection, able to incorporate with a high efficiency the 4N1Ks peptide (chemically conjugated to a C18-PEG). In this way, the peptide's C18 chain was incorporated in the lipidic carrier structure, while the peptide was exposed on its surface being available for senescent cells targeting. Extensive physicochemical characterization shows that the dialysis purification method did not impair the nanosystems features and that these present a small particle size and are stable in different biological media. SNs-Ks demonstrated a higher internalization by cancer cells in comparison to the blank nanosystems. In addition, SNs improved 4N1Ks senolytic activity lowering its effective dose to impair cancer and senescent cancer cells' capacity to proliferate and form colonies. Considering the results presented in this work, next steps will involve further investigation of the therapeutic effect of SNs-Ks *in vivo*.

CRediT authorship contribution statement

Raneem Jatal: Conceptualization, Methodology, Software, Validation, Formal analysis, Investigation, Data curation, Writing – original draft. **Sofia Mendes Saraiva:** Methodology, Software, Validation, Formal analysis, Investigation, Data curation, Writing – original draft, Visualization. **Carlos Vázquez-Vázquez:** Methodology, Software, Validation, Formal analysis, Investigation, Writing – review & editing. **Eric Lelievre:** Methodology, Formal analysis, Investigation. **Olivier Coqueret:** Conceptualization, Investigation, Resources, Supervision, Funding acquisition. **Rafael López-López:** Project administration, Funding acquisition. **Maria de la Fuente:** Conceptualization, Investigation, Resources, Writing – review & editing, Supervision, Project administration, Funding acquisition.

Declaration of Competing Interest

The authors declare the following financial interests/personal relationships which may be considered as potential competing interests: Rafael Lopez Lopez reports a relationship with Roche, AstraZeneca, Merck, MSD, Bayer, BMS, Novartis, Janssen, Lilly, Pfizer, Leo, Rovi, Daiichi Sankyo, Seattle Genetics and Pharmamar that includes: consulting or advisory. Rafael Lopez Lopez reports a relationship with Nasasbiotech, S.L. that includes: board membership and equity or stocks. M.d. l.F is co-founder, shareholder and CEO of DIVERSA Technologies S.L..

Acknowledgements

This work was funded by Instituto de Salud Carlos III (ISCIII) and European Regional Development Fund (FEDER) (PI18/00176), and by the Axencia Galega de Coñecemento en Saúde (GAIN), Xunta de Galicia (IN607B2021/14). NANOMAG group belongs to Galician Competitive Research Group (GRC) (ED431C-2021/16), co-funded by FEDER (EU). R.J. also acknowledges the European financial support in the frame of

the NanoFar program, an Erasmus Mundus Joint Doctorate program in nanomedicine and pharmaceutical innovation.

R.L.-L. performs the role of advisor for Roche, AstraZeneca, Merck, MSD, Bayer, BMS, Novartis, Janssen, Lilly, Pfizer, Leo, Rovi, Daiichi Sankyo and Seattle Genetics; research support for Roche and Merck; reports personal fees from Roche, Novartis and Pharmamar, outside the submitted work; Co-founder and shareholder of Nasasbiotech, S.L..

M.d.l.F is co-founder, shareholder and CEO of DIVERSA Technologies S.L..

The other authors declare no conflict of interest.

Data and materials availability

All data from this study are shown in the paper. The raw data required to reproduce these findings are available from the corresponding authors upon reasonable request.

References

Acosta, J.C., Gil, J., 2012. Senescence: A new weapon for cancer therapy. Trends Cell Biol. 22 (4), 211–219. https://doi.org/10.1016/j.tcb.2011.11.006.

Agostini, A., Mondragón, L., Bernardos, A., Martínez-Máñez, R., Marcos, M.D., Sancenón, F., Soto, J., Costero, A., Manguan-García, C., Perona, R., Moreno-Torres, M., Aparicio-Sanchis, R., Murguía, J.R., 2012. Targeted cargo delivery in senescent cells using capped mesoporous silica nanoparticles. Angew. Chemie - Int. Ed. 51 (42), 10556–10560. https://doi.org/10.1002/anie.201204663.

Aramesh, M., Shimoni, O., Ostrikov, K., Prawer, S., Cervenka, J., 2015. Surface charge effects in protein adsorption on nanodiamonds. Nanoscale 7 (13), 5726–5736. https://doi.org/10.1039/C5NR00250H.

Belcastro, E., Rehman, A.U., Remila, L., Park, S.-H., Gong, D.S., Anton, N., Auger, C., Lefebvre, O., Goetz, J.G., Collot, M., Klymchenko, A.S., Vandamme, T.F., Schini-Kerth, V.B., 2021. Fluorescent nanocarriers targeting VCAM-1 for early detection of senescent endothelial cells. Nanomedicine 34, 102379. https://doi.org/10.1016/j.nano.2021.102379.

Berrecoso, G., Crecente-Campo, J., Alonso, M.J., 2020. Unveiling the pitfalls of the protein corona of polymeric drug nanocarriers. Drug Deliv. Transl. Res. 10 (3), 730–750.

Borghesan, M., Hoogaars, W.M.H., Varela-Eirin, M., Talma, N., Demaria, M., 2020. A Senescence-Centric View of Aging: Implications for Longevity and Disease. Trends Cell Biol. 30 (10), 777–791. https://doi.org/10.1016/j.tcb.2020.07.002.

Bouzo, B.L., 2019. Design and Evaluation of Sphingomyelin Nanosystems for the Development of Anticancer Targeted Therapies. Universidad de Santiago de Compostela.

Bouzo, B.L., Calvelo, M., Martín-Pastor, M., García-Fandiño, R., de la Fuente, M., 2020. In vitro- in silico modeling approach to rationally designed simple and versatile drug delivery systems. J. Phys. Chem. B 124 (28), 5788–5800. https://doi.org/10.1021/acs.jpcb.0c02731.

Bouzo, B.L., Lores, S., Jatal, R., Alijas, S., Alonso, M.J., Conejos-Sánchez, I., de la Fuente, M., 2021. Sphingomyelin nanosystems loaded with uroguanylin and etoposide for treating metastatic colorectal cancer. Sci. Rep. 11, 1–12. https://doi.org/10.1038/s41598-021-96578-z.

Bruno, B.J., Miller, G.D., Lim, C.S., 2013. Basics and recent advances in peptide and protein drug delivery. Ther. Deliv 4 (11), 1443–1467. https://doi.org/10.4155/tde.13.104.

Chung, E.J., 2016. Targeting and therapeutic peptides in nanomedicine for atherosclerosis. Exp. Biol. Med. 241 (9), 891–898. https://doi.org/10.1177/1535370216640940.

Díez-Villares, S., Pellico, J., Gómez-Lado, N., Grijalvo, S., Alijas, S., Eritja, R., Herranz, F., Aguiar, P., de la Fuente, M., 2021. Biodistribution of 68/67Ga-Radiolabeled Sphingolipid Nanoemulsions by PET and SPECT Imaging. Int. J. Nanomed. 16, 5923–5935. https://doi.org/10.2147/IJN.S316767.

Díez-Villares, S., Ramos-Docampo, M.A., da Silva-Candal, A., Hervella, P., Vázquez-Ríos, A.J., Dávila-Ibáñez, A.B., López-López, R., Iglesias-Rey, R., Salgueiriño, V., Fuente, M.d.l., 2021. Manganese Ferrite Nanoparticles Encapsulated into Vitamin E/Sphingomyelin Nanoemulsions as Contrast Agents for High-Sensitive Magnetic Resonance Imaging. Adv. Healthc. Mater. 10 (21), 2101019. https://doi.org/10.1002/adhm.202101019.

Dobrovolskaia, M.A., Clogston, J.D., Neun, B.W., Hall, J.B., Patri, A.K., McNeil, S.E., 2008. Method for analysis of nanoparticle hemolytic properties in vitro. Nano Lett. 8 (8), 2180–2187. https://doi.org/10.1021/nl0805615.

Durán-Lobato, M., López-Estévez, A.M., Cordeiro, A.S., Dacoba, T.G., Crecente-Campo, J., Torres, D., Alonso, M.J., 2021. Nanotechnologies for the delivery of biologicals: Historical perspective and current landscape. Adv. Drug Deliv. Rev. 176, 113899. https://doi.org/10.1016/j.addr.2021.113899.

Ekpenyong-Akiba, A.E., Canfarotta, F., Abd, B., Poblocka, M., Casulleras, M., Castilla-Vallmanya, L., Kocsis-Fodor, G., Kelly, M.E., Janus, J., Althubiti, M., Piletska, E., Piletsky, S., Macip, S., 2019. Detecting and targeting senescent cells using molecularly imprinted nanoparticles. Nanoscale Horiz. 4 (3), 757–768. https://doi.org/10.1039/C8NH00473K.

Fakhari, A., Baoum, A., Siahaan, T.J., Le, K.B., Berkland, C., 2011. Controlling ligand surface density optimizes nanoparticle binding to ICAM-1. J. Pharm. Sci. 100 (3), 1045–1056. https://doi.org/10.1002/jps.22342.

Filipe, V., Hawe, A., Jiskoot, W., 2010. Critical evaluation of Nanoparticle Tracking Analysis (NTA) by NanoSight for the measurement of nanoparticles and protein aggregates. Pharm. Res. 27 (5), 796–810. https://doi.org/10.1007/s11095-010-0073-2.

Forest, V., Cottier, M., Pourchez, J., 2015. Electrostatic interactions favor the binding of positive nanoparticles on cells: A reductive theory. Nano Today 10 (6), 677–680. https://doi.org/10.1016/j.nantod.2015.07.002.

Fornaguera, C., Solans, C., 2017. Methods for the in vitro characterization of nanomedicines—biological component interaction. J. Pers. Med. 7 (1), 2. https://doi.org/10.3390/jpm7010002.

Fosgerau, K., Hoffmann, T., 2015. Peptide therapeutics: Current status and future directions. Drug Discov. Today 20 (1), 122–128. https://doi.org/10.1016/j.drudis.2014.10.003.

Franken, N.A.P., Rodermond, H.M., Stap, J., Haveman, J., van Bree, C., 2006. Clonogenic assay of cells in vitro. Nat. Protoc. 1 (5), 2315–2319. https://doi.org/10.1038/nprot.2006.339.

Gao, H., Yang, Z., Zhang, S., Cao, S., Shen, S., Pang, Z., Jiang, X., 2013. Ligand modified nanoparticles increases cell uptake, alters endocytosis and elevates glioma distribution and internalization. Sci. Rep. 3, 2534. https://doi.org/10.1038/SREP02534.

Guillon, J., Petit, C., Moreau, M., Toutain, B., Henry, C., Roché, H., Bonichon-Lamichhane, N., Salmon, J.P., Lemonnier, J., Campone, M., Verrièle, V., Lelièvre, E., Guette, C., Coqueret, O., 2019. Regulation of senescence escape by TSP1 and CD47 following chemotherapy treatment. Cell Death Dis. 10 (3) https://doi.org/10.1038/s41419-019-1406-7.

de la Harpe, K., Kondiah, P., Choonara, Y., Marimuthu, T., du Toit, L., Pillay, V., 2019. The Hemocompatibility of Nanoparticles: A Review of Cell-Nanoparticle Interactions and Hemostasis. Cells 8 (10), 1209. https://doi.org/10.3390/cells8101209.

Jatal, R., Lelievre, E., Coqueret, O., 2021. TSP-1 C-terminal derived peptide and its effect on chemotherapy-induced senescence (submitted for publication).

Jeong, W., Bu, J., Kubiatowicz, L.J., Chen, S.S., Kim, Y.S., Hong, S., 2018. Peptide–nanoparticle conjugates: a next generation of diagnostic and therapeutic platforms? Nano Converg. 5, 1–18. https://doi.org/10.1186/s40580-018-0170-1.

Ke, S., Lai, Y., Zhou, T., Li, L., Wang, Y., Ren, L., Ye, S., 2018. Molybdenum Disulfide Nanoparticles Resist Oxidative Stress-Mediated Impairment of Autophagic Flux and Mitigate Endothelial Cell Senescence and Angiogenic Dysfunctions. ACS Biomater. Sci. Eng. 4 (2), 663–674. https://doi.org/10.1021/acsbiomaterials.7b00714.

Kommuru, T.R., Gurley, B., Khan, M.A., Reddy, I.K., 2001. Self-emulsifying drug delivery systems (SEDDS) of coenzyme Q10: formulation development and bioavailability assessment. Int. J. Pharm. 212 (2), 233–246. https://doi.org/10.1016/S0378-5173(00)00614-1.

Lewinska, A., Adamczyk-Grochala, J., Bloniarz, D., Olszowka, J., Kulpa-Greszta, M., Litwinienko, G., Tomaszewska, A., Wnuk, M., Pazik, R., 2020. AMPK-mediated senolytic and senostatic activity of quercetin surface functionalized Fe3O4 nanoparticles during oxidant-induced senescence in human fibroblasts. Redox Biol. 28, 101337. https://doi.org/10.1016/j.redox.2019.101337.

Milanovic, M., Fan, D.N.Y., Belenki, D., Däbritz, J.H.M., Zhao, Z., Yu, Y., Dörr, J.R., Dimitrova, L., Lenze, D., Monteiro Barbosa, I.A., Mendoza-Parra, M.A., Kanashova, T., Metzner, M., Pardon, K., Reimann, M., Trumpp, A., Dörken, B., Zuber, J., Gronemeyer, H., Hummel, M., Dittmar, G., Lee, S., Schmitt, C.A., 2018. Senescence-associated reprogramming promotes cancer stemness. Nature 553 (7686), 96–100. https://doi.org/10.1038/nature25167.

Mohr, K., Sommer, M., Baier, G., Schöttler, S., Okwieka, P., Tenzer, S., Landfeste, K., Mailänder, V., Schmidt, M., Meyer, G.M., 2014. Aggregation Behavior of Polystyrene-Nanoparticles in Human Blood Serum and its Impact on the in vivo Distribution in Mice. J. Nanomed. Nanotechnol. 5, 193. https://doi.org/10.4172/2157-7439.1000193.

Muñoz-Espín, D., Rovira, M., Galiana, I., Giménez, C., Lozano-Torres, B., Paez-Ribes, M., Llanos, S., Chaib, S., Muñoz-Martín, M., Ucero, A.C., Garaulet, G., Mulero, F., Dann, S.G., VanArsdale, T., Shields, D.J., Bernardos, A., Murguía, J.R., Martínez-Máñez, R., Serrano, M., 2018. A versatile drug delivery system targeting senescent cells. EMBO Mol. Med. 10, 1–18. https://doi.org/10.15252/emmm.201809355.

Muttenthaler, M., King, G.F., Adams, D.J., Alewood, P.F., 2021. Trends in peptide drug discovery. Nat. Rev. Drug Discov. 20 (4), 309–325. https://doi.org/10.1038/s41573-020-00135-8.

Nagachinta, S., Becker, G., Dammicco, S., Serrano, M.E., Leroi, N., Bahri, M.A., Plenevaux, A., Lemaire, C., Lopez, R., Luxen, A., de la Fuente, M., 2020a. Radiolabelling of lipid-based nanocarriers with fluorine-18 for in vivo tracking by PET. Colloids Surfaces B Biointerfaces 188, 110793. https://doi.org/10.1016/j.colsurfb.2020.110793.

Nagachinta, S., Bouzo, B.L., Vazquez-Rios, A.J., Lopez, R., de la Fuente, M., 2020b. Sphingomyelin-based nanosystems (SNs) for the development of anticancer miRNA therapeutics. Pharmaceutics 12, 189. https://doi.org/10.3390/pharmaceutics12020189.

Paez-Ribes, M., González-Gualda, E., Doherty, G.J., Muñoz-Espín, D., 2019. Targeting senescent cells in translational medicine. EMBO Mol. Med. e10234 https://doi.org/10.15252/emmm.201810234.

Pudlarz, A., Szemraj, J., 2018. Nanoparticles as carriers of proteins, peptides and other therapeutic molecules. Open Life Sci. 13, 285–298. https://doi.org/10.1515/biol-2018-0035.

Rasband, W.S., n.d. ImageJ, U. S. National Institutes of Health, Bethesda, Maryland, USA, https://imagej.nih.gov/ij/, 1997–2018.

Ruozi, B., Tosi, G., Forni, F., Fresta, M., Vandelli, M.A., 2005. Atomic force microscopy and photon correlation spectroscopy: Two techniques for rapid characterization of liposomes. Eur. J. Pharm. Sci. 25 (1), 81–89. https://doi.org/10.1016/j.ejps.2005.01.020.

Saberi, A.H., Fang, Y., McClements, D.J., 2013. Fabrication of vitamin E-enriched nanoemulsions: Factors affecting particle size using spontaneous emulsification. J. Colloid Interface Sci. 391, 95–102. https://doi.org/10.1016/J.JCIS.2012.08.069.

Saleh, T., Tyutyunyk-Massey, L., Gewirtz, D.A., 2019. Tumor cell escape from therapy-induced senescence as a model of disease recurrence after dormancy. Cancer Res. 79 (6), 1044–1046. https://doi.org/10.1158/0008-5472.CAN-18-3437.

Solaro, R., Chiellini, F., Battisti, A., 2010. Targeted Delivery of Protein Drugs by Nanocarriers. Materials (Basel) 3 (3), 1928–1980. https://doi.org/10.3390/ma3031928.

Thapa, R.K., Nguyen, H.T., Jeong, J.H., Kim, J.R., Choi, H.G., Yong, C.S., Kim, J.O., 2017. Progressive slowdown/prevention of cellular senescence by CD9-targeted delivery of rapamycin using lactose-wrapped calcium carbonate nanoparticles. Sci. Rep. 7, 1–11. https://doi.org/10.1038/srep43299.

Therapeutic Proteins Global Market Report 2021: COVID-19 Impact and Recovery to 2030 [WWW Document], n.d. URL https://www.businesswire.com/news/home/20210615005937/en/Therapeutic-Proteins-Global-Market-Report-2021-COVID-19-Impact-and-Recovery-to-2030—ResearchAndMarkets.com (accessed 8.1.21).

Wang, L., Dong, J., Chen, J., Eastoe, J., Li, X., 2009. Design and optimization of a new self-nanoemulsifying drug delivery system. J. Colloid Interface Sci. 330 (2), 443–448.

Weber, M., Steinle, H., Golombek, S., Hann, L., Schlensak, C., Wendel, H.P., Avci-Adali, M., 2018. Blood-Contacting Biomaterials. In Vitro Evaluation of the Hemocompatibility. Front. Bioeng. Biotechnol. 6, 99. https://doi.org/10.3389/FBIOE.2018.00099/BIBTEX.

Wissler Gerdes, E.O., Zhu, Y.i., Tchkonia, T., Kirkland, J.L., 2020. Discovery, development, and future application of senolytics: theories and predictions. FEBS J. 287 (12), 2418–2427. https://doi.org/10.1111/febs.15264.

Wu, L., Zhang, J., Watanabe, W., 2011. Physical and chemical stability of drug nanoparticles. Adv. Drug Deliv. Rev. 63 (6), 456–469. https://doi.org/10.1016/j.addr.2011.02.001.

Yang, L., Fang, J., Chen, J., 2017. Tumor cell senescence response produces aggressive variants. Cell Death Discov. 3, 1–11. https://doi.org/10.1038/cddiscovery.2017.49.

Zhu, Y.i., Tchkonia, T., Pirtskhalava, T., Gower, A.C., Ding, H., Giorgadze, N., Palmer, A.K., Ikeno, Y., Hubbard, G.B., Lenburg, M., O'Hara, S.P., LaRusso, N.F., Miller, J.D., Roos, C.M., Verzosa, G.C., LeBrasseur, N.K., Wren, J.D., Farr, J.N., Khosla, S., Stout, M.B., McGowan, S.J., Fuhrmann-Stroissnigg, H., Gurkar, A.U., Zhao, J., Colangelo, D., Dorronsoro, A., Ling, Y.Y., Barghouthy, A.S., Navarro, D.C., Sano, T., Robbins, P.D., Niedernhofer, L.J., Kirkland, J.L., 2015. The Achilles' heel of senescent cells: from transcriptome to senolytic drugs. Aging Cell 14 (4), 644–658. https://doi.org/10.1111/acel.12344.